# Wave energy focusing in a three-dimensional numerical wave tank

Christophe Fochesato, Frédéric Dias, and Stephan Grilli

[1] MAB, Université de Bordeaux,
351 Cours de la Libération, 33405 Talence cedex, France
Christophe.Fochesato@math.u-bordeaux1.fr
[2] CMLA, ENS Cachan,
61, avenue du Président Wilson, 94235 Cachan cedex, France
Frederic.Dias@cmla.ens-cachan.fr
[3] Department of Ocean Engineering,
University of Rhode Island, Narragansett, RI 02882, USA
grilli@oce.uri.edu

**Abstract.** Extreme waves are obtained from the motion of a snake wavemaker in a numerical wave tank. Spatial focusing is one of the mechanisms which may take part in the generation of a rogue wave. In particular, directional focusing is only a three-dimensional phenomenon, that we want to isolate in this study. The numerical model solves incompressible Euler equations with a free surface for a potential flow, thanks to a Boundary Element Method and a mixed Eulerian-Lagrangian time updating. Its more recent improvement has consisted in the insertion of the fast multipole algorithm in order to reduce the computational complexity of the spatial solver. We present a typical case of a near breaking rogue wave. A description of the particular geometry of such a wave is discussed, as well as the kinematics at the surface.

## Introduction

The general framework is the study of the rare but important phenomenon that are the freak waves. Indeed, in spite of their low probability of occurrence, these waves can cause severe damages and the off-shore and naval communities must take into account such events for their design rules. Besides their low probability, freak waves are characterized by the fact that they are localized in time as well as in space. They come from some energy focusing, which can be due to multiple reasons. Spatial focusing is one of the mechanisms, commonly proposed to explain the appearance of a rogue wave. More generally, linear theory suggests that different wave components can have different phase and directions, so that they superimpose in a small region of space and time. Actually, energy focusing may come from another reason. It can result from the bottom topography in shallow water, or from wave-current interactions. In deep water and without the presence of a current, a more recent proposed mechanism is the modulational instability (Benjamin-Feir instability). Lastly, other wave-wave interactions or interactions

with atmospheric conditions may play a role in the phenomenon. These mechanisms are summed up in the recent review article by Kharif and Pelinovsky [10].

If most of works on rogue waves concern deep water, it has been remarked that it can occur for any water depth. In the present study, we consider finite depth, but specifying a flat bottom in order to concentrate only on one focusing mechanism. Spatial focusing is the natural mechanism to generate extreme waves in laboratory. It is a controlled context which represents the superposition of several sinusoidal wave components. The first possibility is frequential focusing which occurs when faster waves catch again slower ones, generated earlier. That is how two-dimensional studies have been carried out. Directional focusing is uniquely a three-dimensional phenomenon. In order to generate it, a snake wavemaker can be used to give several swells which cross at one point of the basin. She *et al.* [11] made such laboratory experiments and studied the kinematics of breaking waves thanks to the PIV technique. Brandini and Grilli [4, 2] adapted the Boundary Element code of [9] by inserting a snake wavemaker, and started a numerical study on spatial focusing. More recently, Bonnefoy *et al.* [1] developped a numerical tool based on a spectral solving of Euler's equation with a free surface and undertook to compare with some experiments. Their method allows to consider more wave components in a larger basin, with a random-like waves field, the wave components propagating as wave packets. Then, they can reproduce a focusing wave event, close to one coming from a sea state. Nevertheless from the numerical point of view, their calculations are limited by the nature of the method used, and they cannot pursue until wave overturning. The present study arises in a lightly different context. Indeed, the aim consists in isolating the phenomenon of directional focusing which leads to a breaking wave in order to study their kinematics. It comes in the following of Grilli and Brandini's work [4] on the use of a Boundary Element Method to solve Euler equations with a free surface. The main drawbacks of this kind of discretization is its computational cost, which is quadratic with the number of nodes used to mesh the whole boundary of the domain. This obstacle has been got over with the insertion of the fast multipole algorithm in order to speed up all the matrix-vector products in the spatial solver [7]. The next section presents the numerical method and its more recent improvement. Then the configuration of the tank is described. Last, the results are discussed in section four.

## Numerical model

We consider the equations for a potential flow of a perfect, incompressible fluid, with a free surface. Inside the domain, they reduce to the Laplace equation

$$\Delta\phi = 0$$

for the velocity potential $\phi$, defined from the velocity $\boldsymbol{u} = \boldsymbol{\nabla}\phi$. Green's second identity transforms this equation into a Boundary Integral Equation (BIE) on

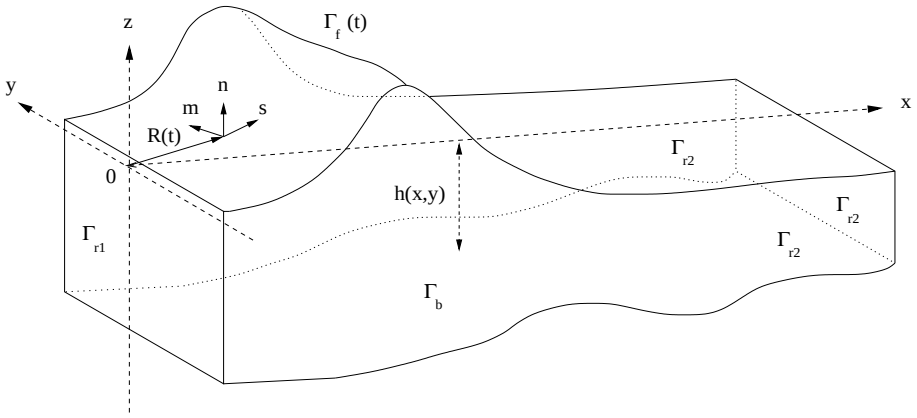


**Fig. 1.** Domain of computation. The free surface $\Gamma_f(t)$ is defined at each time step by the position vector $\boldsymbol{R}(t)$. Lateral boundaries are denoted by $\Gamma_{r1}$ and $\Gamma_{r2}$. The bottom $\Gamma_b$ is defined by $z = h(x, y)$. Use is made of the Cartesian coordinate system $(x, y, z)$ and of the local curvilinear coordinate system $(s, m, n)$, defined at the point $\boldsymbol{R}(t)$ of the boundary.

the boundary

$$\alpha(\boldsymbol{x}_l)\,\phi(\boldsymbol{x}_l) = \int_{\Gamma(t)} \left\{ \frac{\partial \phi}{\partial n}(\boldsymbol{x})\, G(\boldsymbol{x}, \boldsymbol{x}_l) - \phi(\boldsymbol{x})\, \frac{\partial G}{\partial n}(\boldsymbol{x}, \boldsymbol{x}_l) \right\} \mathrm{d}\Gamma, \tag{1}$$

where $G(\boldsymbol{x}, \boldsymbol{x}_l) = 1/4\pi|\boldsymbol{x} - \boldsymbol{x}_l|$ is the Green's function for the 3D free space,$\boldsymbol{n}$ is the normal vector exterior to the boundary and $\alpha(\boldsymbol{x}_l)$ is proportional to the solid exterior angle made by the boundary at the collocation point $\boldsymbol{x}_l$. On the free surface, the potential $\phi$ satisfies the nonlinear kinematic and dynamic boundary conditions

$$\frac{D\,\boldsymbol{R}}{D\,t} = \boldsymbol{\nabla}\phi, \tag{2}$$

$$\frac{D\,\phi}{D\,t} = -gz + \frac{1}{2}\,\boldsymbol{\nabla}\phi \cdot \boldsymbol{\nabla}\phi, \tag{3}$$

where $\boldsymbol{R}$ is the position vector of a fluid particle on the free surface, $g$ the acceleration due to gravity and $D/Dt$ the material derivative. Lateral boundaries are either fixed or moving boundaries. In the first case, the potential is specified on the free surface in order to determine the initial perturbation. In the second case, waves are generated by a wavemaker at the open boundary, $\Gamma_{r1}(t)$, the motion $\boldsymbol{x}_p$ and velocity $\boldsymbol{u}_p$ being specified as

$$\overline{\boldsymbol{x}} = \boldsymbol{x}_p \; and \; \overline{\frac{\partial \phi}{\partial n}} = \boldsymbol{u}_p \cdot \boldsymbol{n}$$

where overlines denote specified values. Along the fixed parts of the boundary, the no-flow condition is prescribed:

$$\overline{\frac{\partial \phi}{\partial n}} = 0.$$

The domain represents a closed basin such as a wave tank, whose bottom can be defined with arbitrary shape. The numerical model is presented in details in Grilli *et al.* [9]. The time scheme consists in updating the position vector and the velocity potential on the free surface based on second order Taylor expansions. At each time step, The BIE must be solved which is realized through the Boundary Element Method. The boundary is divided into elements for which a local interpolation is defined, both for the geometry and field variables. Polynomial shape functions are introduced, that also define a change of variables which brings the integrations on a cartesian reference element. The numerical computation of these integrals by a Gauss-Legendre quadrature and appropriate techniques for singularities of the Green's functions make up the assembling phase of the discretization matrix. This one is modified by taking into account the rigid mode technique which allows to directly compute the solid angles and to avoid the singular integrations of the normal derivative of the Green's function. The insertion of the multiple node technique in order to deal with the edges also leads to a modification of the matrix. Lastly, the velocity potential, or its normal derivative depending on the boundary, is obtained by solving the resulting linear system. Since the matrix is full, the method has a $N^2$ computational complexity, where $N$ is the number of nodes, by using the iterative algorithm GMRES so that the solving phase be at the same level as the assembling phase. In order to reduce this complexity, the fast multipole algorithm is inserted. The idea is to replace every matrix-vector product coming from the discretization of the BIE by a call to this algorithm.

This one lies on a property of the Green's function which can be expanded in separate variables when the source point and the evaluation point are far enough from each other. It can then be written for a point $O$, origin of the expansion, close to $\boldsymbol{x}$ and far from $\boldsymbol{x}_l$

$$G(\boldsymbol{x}, \boldsymbol{x}_l) \approx \frac{1}{4\pi} \sum_{k=0}^{p} \sum_{m=-k}^{k} \rho^k Y_k^{-m}(\alpha, \beta) \frac{Y_k^m(\theta, \varphi)}{r^{k+1}}, \tag{4}$$

where $O\boldsymbol{x} = (\rho, \alpha, \beta)$ and $O\boldsymbol{x}_l = (r, \theta, \varphi)$ in spherical coordinates, and the functions $Y_k^{\pm m}$ are the spherical harmonics defined from the Legendre polynomials. In order to determine in what cases this new approximation can be used, a hierarchical subdivision of space is defined, whose regular partitioning automatically gives distance criteria. Then, close interactions are obtained by direct computation with Green's functions, whereas far interactions can be approximated by successive local operations based on the subdivision into cells and expansions of the Green' functions into spherical harmonics. The underlying theory to this

approximation has been well established in the case of the Laplace's equation. In particular, error and complexity analysis are given in the monograph by Greengard [8].

In our case, the Laplace's equation has been transformed into an integral equation and a specific discretization has been used. Thus, the fast algorithm must be adapted in order to be part of the surface wave model, but the expansions remain the same. The integral equation can be written as

$$\alpha(\boldsymbol{x}_l)\,\phi(\boldsymbol{x}_l) \approx \frac{1}{4\pi} \sum_{k=0}^{p} \sum_{m=-k}^{k} M_k^m(O) \frac{Y_k^m(\theta,\varphi)}{r^{k+1}}, \tag{5}$$

where $M_k^m(O)$ is the moment at the origin $O$:

$$M_k^m(O) = \int_\Gamma \left\{ \frac{\partial \phi}{\partial n}(\boldsymbol{x})\, \rho^k Y_k^{-m}(\alpha,\beta) - \phi(\boldsymbol{x})\, \frac{\partial}{\partial n}\left( \rho^k Y_k^{-m}(\alpha,\beta) \right) \right\} \mathrm{d}\Gamma. \tag{6}$$

Instead of considering mutual interactions between two points, we need to look at the contribution of an element of the discretization to a collocation point. The local computation of several elements grouped together into a multipole calls on a boundary element analysis with the spherical harmonics instead of the Green's function. The integration of the normal derivative of the spherical harmonics is done by taking care of avoiding an apparent singularity which could generate numerical errors. The discretization by boundary elements only takes place in the computation of the moments. So the rest of the fast multipole algorithm is unchanged, notably for translation and conversion formulas which allow to pass the information through the hierarchical subdivision, from the multipole contributions to the evaluation at every collocation point. From the surface wave model point of view, we have needed to adapt all the aspects depending on the existence of the matrix in the former model. The storage of the coefficients that we want to use several times for each time step is now done inside the cells of the hierarchical subdivision. The rigid mode and multiple nodes techniques modified the matrix *a priori* before the computation of the matrix-vector products. They are now considered as correction terms to the result of such products, so that the linear system to be solved keeps the same properties.

The accelerated model only benefits from a faster solver for the Laplace equation at each time step. It has been tested by comparing with the former model on a three-dimensional application which requires a great accuracy. It is the propagation of a solitary wave on a sloping bottom with a transverse modulation which leads to a plunging jet. Above all, the consistency of the new approximation has been checked up. But, what is important is that the accuracy and stability are not distorted. By adjusting the parameters of the fast multipole algorithm, it is possible to get the same result as with the former model. In this case, the computing times evolves nearly linearly with the number of nodes, above roughly 4000 nodes.

## Description of the tank

A rectangular basin with a flat bottom is defined. It is limited by fixed and moving boundaries. At one extremity, a snake wavemaker has been implemented [4]. It is a rotating wavemaker whose axis is located at the bottom, at depth $h_0$. It is composed of several vertical parts which can move independently. The position $\boldsymbol{x}_p = (x_p, y_p, z_p)$ of each vertical part is defined by

$$\boldsymbol{x}_p = \boldsymbol{x}_o - \rho\,\boldsymbol{m} \quad \text{, with} \quad \boldsymbol{x}_o = y_p\,\boldsymbol{j} - h_o\,\boldsymbol{k} \tag{7}$$

the coordinates of the paddle axis rotation, where the angular velocity $\dot{\Omega}\,\boldsymbol{j}$ is applied. We denote $\rho$ the distance fron the axis of rotation, measured on the wavemaker in vertical planes. Hence,

$$\rho = \sqrt{x_p^2 + (h_o + z_p)^2} \quad \text{, and} \quad \Omega = \arctan\frac{S_o}{h_o} \tag{8}$$

where $S_o(y,t)$ corresponds to the horizontal stroke specified at $z = 0$. From these definitions, we find the velocity and acceleration vectors

$$\begin{aligned} \boldsymbol{u}_p &= -\dot{\rho}\,\boldsymbol{m} - \rho\,\dot{\Omega}\,\boldsymbol{n} \\ \frac{\mathrm{d}\boldsymbol{u}_p}{\mathrm{d}t} &= (\rho\,\dot{\Omega}^2 - \ddot{\rho})\,\boldsymbol{m} - (2\,\dot{\rho}\,\dot{\Omega} + \rho\,\ddot{\Omega})\,\boldsymbol{n}. \end{aligned} \tag{9}$$

Following Dalrymple [6], we specify the wavemaker stroke $S_o$ as the linear superposition of $N_\theta$ sinusoidal components of amplitude $a_n$ and direction $\theta_n$, as

$$S_o(y,t) = \sum_{n=1}^{N_\theta} a_n \cos\left\{k_n\left(y\sin\theta_n - x_f\cos\theta_n\right) - \omega_n t\right\} \tag{10}$$

where $k_n$ and $\omega_n$ denote components' wavenumber and wave frequency, related by the linear dispersion relationship

$$\omega_n^2 = g\,k_n\,\tanh\left(k_n h_o\right) \tag{11}$$

and $x_f$ is the focusing distance for the waves in front of the wavemaker. Angles $\theta_n$ are uniformly distributed in the range $[-\theta_{\max}, \theta_{\max}]$. Only directionnal focusing is studied here, hence $\omega_n = \omega$. Frequential focusing could be added by adjusting the frequency as a function of the angle $\theta_n$. Moreover, we restrict ourselves to the case where the amplitudes are the same, but different values could be chosen.

The first objective of this work has consisted in looking for a parameter set such that a breaking wave is generated. We consider the superposition of eight components having identical properties but with directions comprised between $-45$ and 45 degrees. Variables being non-dimensionalized (length by the water depth $h_0$, and time by $\sqrt{h_0/g}$), every component is determined by a frequency 1.2816 which gives a wavelength 3.725 after the dispersion relationship and a linear velocity $c = 0.7599$. The shared amplitude of each individual component

is fixed to 0.04 implying the steepness 0.0675. Last, the focusing point is specified at the distance 7.5 from the wavemaker. Once defined the features of the wave field, the dimensions of the tank are adapted. Length is chosen at 10 and width at 20. The discretization uses 50 elements in the longitudinal direction, what corresponds to roughly 20 nodes per wavelength. The width of thee domain is divided into 70 elements, and the depth into 4 elements. Note that all the boundaries are discretized. the presented simulation has been obtained in 4min 30s per time step with an Intel Pentium 4 processor, for more than 300 time steps.

To illustrate, Figure 2 presents the kind of movement executed by the wavemaker. At the other extremity of the domain, an absorbing piston is used [5, **?**]. Though it is not perfectly adapted to this three-dimensional waves, it delays the moment when reflection cannot be neglected any more. The implementation of a piston having the same kind of movement as the snake wavemker would improve this feature.

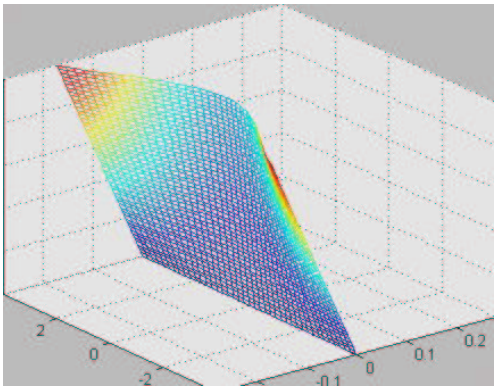


**Fig. 2.** Illustration of the snake movement of the wavemaker located at the left of the tank.

## Results

Figures 4 and 5 present the time evolution of the wave field. Note that only the free surface is shown. The wavemaker progressively sets out in order to reduce the singularities at the interface between the free surface and the moving boundary [4]. We observe the flat free surface at rest which starts to move near the wavemaker and generates a first focused wave of moderate amplitude (Figure 4). Then, the wave amplitude diminishes before disappearing at the graph scale (Figure 5). The studied mechanism effectively produces some local focusing both in time and space. Behind this first wave, we can see a second one which clearly

results from the superposition of the wave components with different directions (Figure 5(b),(c)). The amplitude of the wavemaker oscillations incrreases and the sum of the wave components gives rise to an extreme wave in the middle of the tank (Figure 5(d),(e)). This one steepens before reaching the focus point, foreseen at $x = 7.5$. At the end time of the simulation, the crest is located at $x = 4.4$ (Figure 5(f)). Behind, we remark that the phenomenon was starting to be repeated with a new curved crest line converging to the center of the basin.

The observation of the free surface shape for this three-dimensional application leads to the following comments. First of all, we see a circular trough located just in front of the wave. Behind it, a deeper trough has formed, separating the main wave from the curved crest line which follows it. This trough has a crescent shape. A strong asymetry between back and front of the wave is observed. Its amplitude is significatively greater than following waves which have not yet converged. This asymetry increases along time and indicates that the wave is about to break. The wave itself appears like a curved front. In the present case where the directionality is important, the front is not so wide and three-dimensional effects are emphasized (though noting that axis are not at real scales). The observation of this extreme wave presents some geometrical properties found for freak waves. In particular, a vertical slice of the solution at $y = 0$ allows to bring out the shape observed in measured spectra as well as in 2D numerical studies, for instance those about the modulational instability of a wave packet [10]. The crest amplitude is greater than the trough amplitudes, the back trough being deeper (Figure 3). The crest is measured at 0.35, and the back and front troughs are respectively measured at 0.17 and 0.07 (here length unity is the water depth $h_0$). It is remarkable to note that we get such a 2D characteristic shape whereas the mechanism here is only due to the third dimension. This suggests some independence of the wave shape from the causes which generate it.

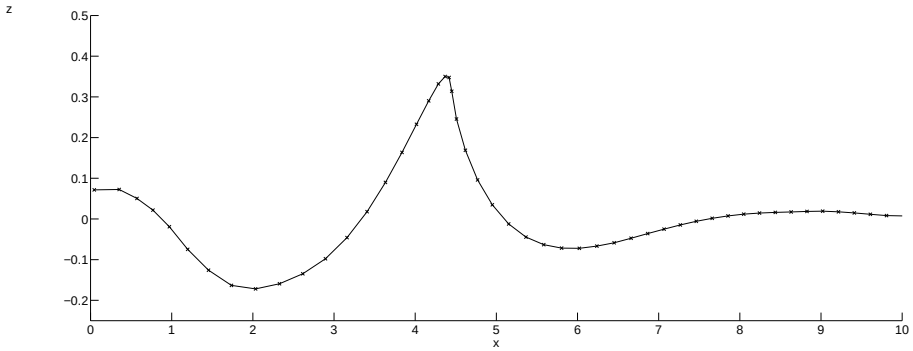


**Fig. 3.** Vertical slice of the free surface at $y = 0$ and $t = 18.308$.

The observation of the velocity and acceleration fields at the free surface shows two main steps in the evolution of this focused wave event. The first step is a phase of approach where the different wave components form a crest line converging to a point. The kinematics simply present the features of the propagation of this curved crest line. The second phase corresponds to the appearance of a unique wave, resulting from the superposition. The maximal value of the longitudinal component of the velocity field increases and the greatest values concentrate more and more at the crest. So this crest tends to go faster forward than the wave basis, what is going to lead to wave breaking. At the same time, the transverse component of the velocity and acceleration fields show that three-dimensional effects are reduced on the front face of the wave. This way, the dynamics of the imminent wave breaking approaches a configuration nearly 2D. This well agrees with some description of "wall of water", that we can find in stories about extreme wave events in the ocean.

## Conclusion

This paper sums up the numerical method we use to study the mechanism of directional focusing in a numerical wave tank. It is based on the solution of incompressible Euler's equations with a free surface for a potential flow, by a Boundary Element Method [9]. Its more recent improvement is presented. It consists in using the Fast Multipole Algorithm in order to compute faster every matrix-vector product coming from the discretization [7]. This allows to overcome the main drawback of such numerical method, that is to say its computational complexity which is $O(N^2)$. The application consists to observe an extreme wave event generated by the movement of a snake wavemaker. Directional focusing is one of the mechanisms which may take part in the generation of a freak wave. This mechanism is only three-dimensional. Following Brandini and Grilli's study [4], we define the conditions of the numerical tank which leads to a breaking extreme wave. The description of such a focused wave is done, but the overturning phase could not be obtained until now. We observe that a 2D vertical slice of the solution looks like the characteristic shape observed for freak waves. Its three-dimensional aspect appears as a curved front with a circular trough in front of the wave and followed by a deeper trough with a crescent shape. The kinematics show two main phases. First, we observe the propagation of a curved crest line converging to one point. When the focused wave is generated, it steepens and the velocity and acceleration vectors on the front face of the wave have a weak transverse component. Therefore, after the focusing phase, the occurence of wave breaking approaches to some dynamics that are essentially two-dimensional. This corresponds to the aspect of "wall of water" which appears in some stories of rogue waves in the ocean. The maximal value of the velocity on the crest just before breaking is measured at $0.73\sqrt{gh_0}$, where $g$ is is the acceleration due to gravity and $h_0$ the depth of the tank at rest.

## References


1. Bonnefoy F., Le Touze D., Ferrant P., Generation of fully-nonlinear prescribed wave fields using a high-order spectral method, Proc. 14th Offshore and Polar Engng. Conf. (ISOPE 2004), Toulon, France, vol. III, 257–263 (2004).
2. Brandini C., Nonlinear interaction processes in extreme wave dynamics, Ph.D. Dissertation, University of Firenze (2001).
3. Brandini C., S.T. Grilli., On the Numerical Modeling of extreme Highly Nonlinear Deep Water Waves, Proc. IABEM 2000 Symposium, Brescia, Italy, 54–58 (2000).
4. Brandini C., Grilli S., Modeling of freak wave generation in a 3D-NWT, Proc. 11th Offshore and Polar Engng. Conf. (ISOPE 2001), Stavanger, Norway, Vol III, 124–131 (2001).
5. Clément A., Coupling of two absorbing boundary conditions for 2D time-domain simulations of free surface gravity waves, *J. Comp. Phys.* **26**, 139–151 (1996).
6. Dalrymple R.A., Directional wavemaker theory with sidewall reflection, *J. Hydraulic Res.* **27** (1), 23–34 (1989).
7. Fochesato C., Dias F., Numerical model using the Fast Multipole Algorithm for nonlinear three-dimensional free-surface waves, prépublication CMLA, 2004.
8. Greengard L., *The Rapid Evaluation of Potential Fields in Particle Systems,* MIT Press, Cambridge, MA, 1988.
9. Grilli S., Guyenne P., Dias F., A fully nonlinear model for three-dimensional overturning waves over arbitrary bottom, *Int. J. Num. Meth. Fluids* **35**, 829–867 (2001).
10. Kharif C., Pelinovsky E., Physical mechanisms of the rogue wave phenomenon, *Eur. J. Mech. B-Fluids* **22** (6), 603–634 (2003).
11. She K., Greated C.A., Easson W.J., Experimental study of three-dimensional wave breaking, *J. of Am. Soc. C. E.* **120**, 20–36 (1994).

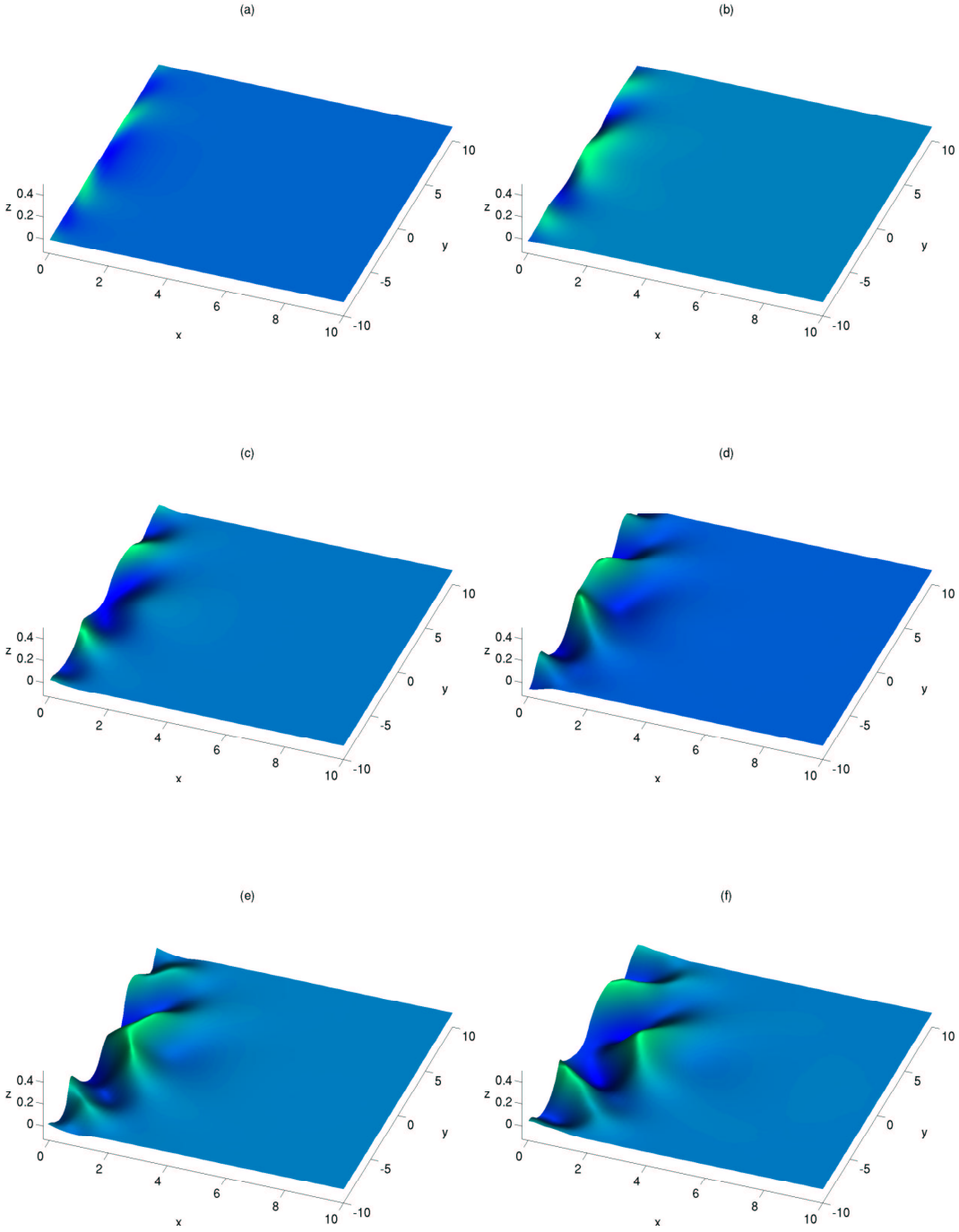


**Fig. 4.** Evolution of the free surface: (a) at $t = 2.143$, (b) at $t = 4.243$, (c) at $t = 6.231$, (d) at $t = 8.025$, (e) at $t = 9.465$, (f) at $t = 10.974$.

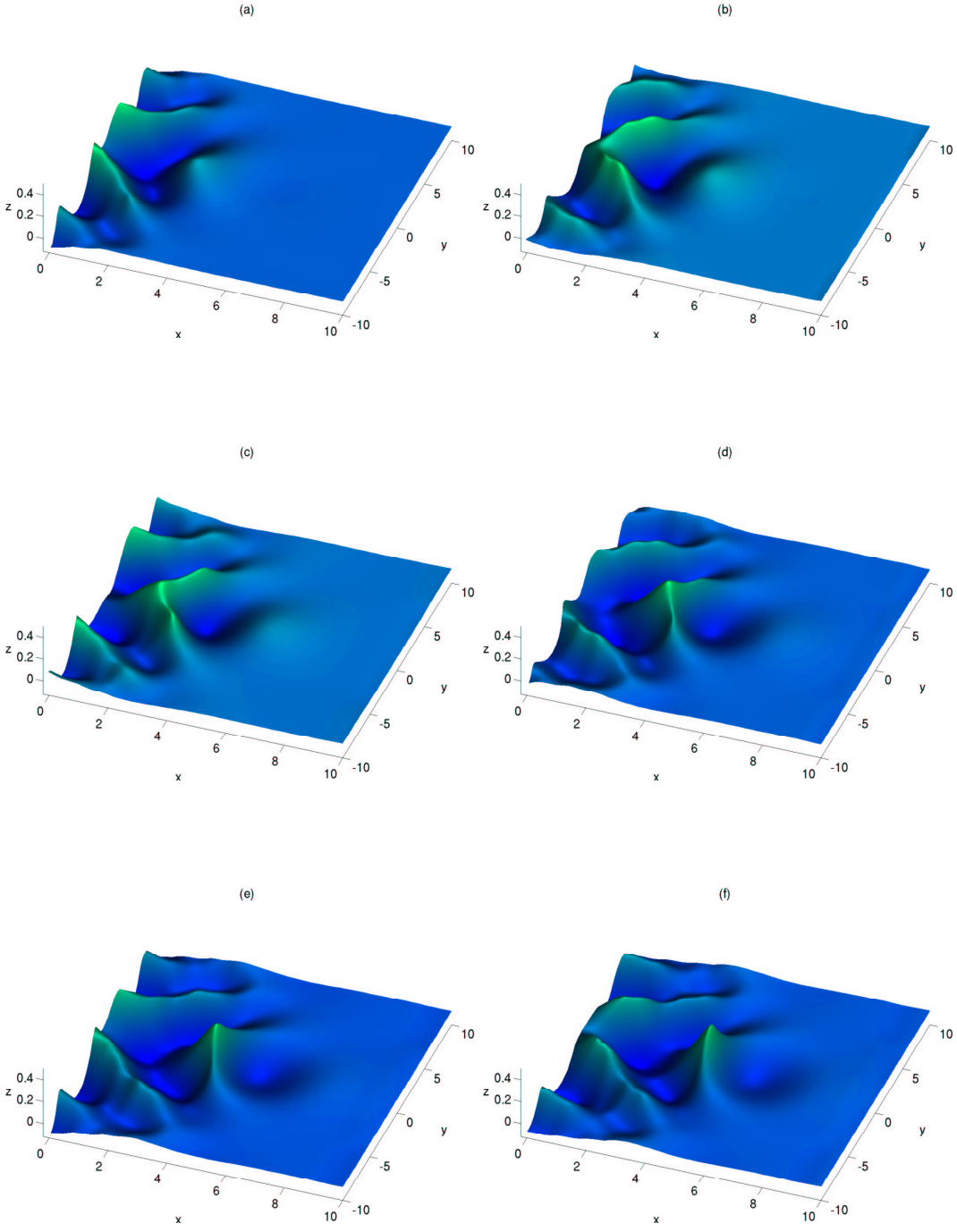


**Fig. 5.** end of the evolution of the free surface: (a) at $t = 12.639$, (b) at $t = 14.077$, (c) at $t = 15.431$, (d) at $t = 16.640$, (e) at $t = 17.650$, (f) at $t = 18.308$.